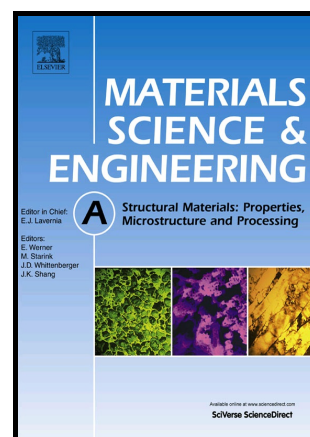# Author's Accepted Manuscript

Oxide dispersion strengthened CoCrFeNiMn high-entropy alloy

Hynek Hadraba, Zdenek Chlup, Antonin Dlouhy, Ferdinand Dobes, Pavla Roupcova, Monika Vilemova, Jiri Matejicek

Cite this article as: Hynek Hadraba, Zdenek Chlup, Antonin Dlouhy, Ferdinand Dobes, Pavla Roupcova, Monika Vilemova and Jiri Matejicek, Oxide dispersion strengthened CoCrFeNiMn high-entropy alloy, *Materials Science & Engineering A,* http://dx.doi.org/10.1016/j.msea.2017.02.068

This is a PDF file of an unedited manuscript that has been accepted for publication. As a service to our customers we are providing this early version of the manuscript. The manuscript will undergo copyediting, typesetting, and review of the resulting galley proof before it is published in its final citable form. Please note that during the production process errors may be discovered which could affect the content, and all legal disclaimers that apply to the journal pertain.

ACCEPTED MANUSCRIPT

Oxide dispersion strengthened CoCrFeNiMn high-entropy alloy

Hynek Hadraba[1*], Zdenek Chlup[1], Antonin Dlouhy[1], Ferdinand Dobes[1], Pavla Roupcova[1], Monika Vilemova[2], Jiri Matejicek[2]

[1]Institute of Physics of Materials, Academy of Sciences of the Czech Republic, Zizkova 22, 616 62 Brno, Czech Republic

[2]Institute of Plasma Physics, Academy of Sciences of the Czech Republic, Za Slovankou 1782/3, 182 00 Praha, Czech Republic

[*]Corresponding author. hadraba@ipm.cz

Abstract

The CoCrFeNiMn high entropy alloy and its strengthened version by in-situ formed dispersion of yttria nano-oxides prepared via mechanical alloying were investigated. The grain refinement of the one phase FCC alloy by presence of oxides was determined by microstructural analyses to be 50%. The positive effect of oxide dispersion on the strength properties was found to be between 30% and 70% for room and elevated temperatures, respectively. The resulting creep strain rates for the strengthened alloy were significantly lower, i.e., three orders for 30MPa stress level, comparing the initial one, therefore, the pining mechanism was among others very effective.

1. Introduction

The concept of high-entropy alloys (HEA) based on multiple principal elements in roughly equal proportions was suggested by Cantor and Yeh [1, 2] in 2004. The main principle of the concept can be pointed in overcoming enthalpies of compounds formation and phase

separation by increased configuration entropy when the number of alloying elements increases [3]. Many researchers have been excited in exploring this new and wide material group; at least 30 elements have been used to prepare more than 300 recently reported HEAs [2, 4, 5]. Although the mechanical response of single phase HEAs is like that of the conventional metals at room temperature when the temperature is lowered to -196°C (liquid nitrogen environment) the yield strength and ultimate tensile strength were found to be simultaneously increasing but accompanied by a decrease of the elongation to the fracture [3]. Compare to other metallic alloys, the fracture toughness of some HEAs is independent on the temperature. Very high fracture toughness of the CoCrFeNiMn HEA was reported at low temperatures (K_{JIc}=219 MPa.m$^{-1/2}$ at -196°C, 221 MPa.m$^{-1/2}$ at -93°C and 217 MPa.m$^{-1/2}$ at 0°C) [6]. Increase in the yield strength, ultimate tensile strength, decrease in elongation to the fracture and high fracture toughness of the CoCrFeNiMn HEA are related to observed change in the deformation mechanism from the conventional dislocation plasticity at room temperature to the nano-twinning at cryogenic temperatures [3]. Deformation mechanisms of the CoCrFeNiMn HEA differ from that of conventional metallic alloys at high temperatures. The highly distorted atomic lattice of this HEA pins dislocations at lower temperatures and prevents thermal vibrations from destroying the pinning effect. When the temperature increases, the alloy displays serrations at a tensile curve caused by avalanches of the dislocation slipping. The serration is a temperature dependent effect whose temperature range depends on the HEA composition, e.g., the CoCrFeNiMn HEA displays serration in the temperature interval 300°C – 620°C. An increase of the number of alloying elements extends the temperature range over which serrations are observed. Binary alloy CoNi has no serration phenomena. The CoFeNi and CoCrFeNi display serration behaviours in the temperature range from 400°C to 500°C and between 300°C and 600°C, respectively [7]. Within the serration temperature interval, the yield strength and the ultimate tensile strength of the HEA substantially decrease due to weakening of the pinning effect [8]. There is a lack of information about creep behaviour of the HEAs. It can be hypothesized that creep behaviour will be also influenced by the serration phenomena. Thanks to their excellent mechanical properties at both low and high temperatures, the high entropy alloys represent a promising alternative structural material for vacuum vessels and for the plasma-facing components of future fusion reactors. The major limitation of the current state-of-the-art fusion structural materials, i.e., ferritic-martensitic steels, is their strength reduction at higher temperatures, which imposes an operation limit of about 500°C – 600°C [9]. The high-temperature embrittlement of ferritic-martensitic steels is generally connected to the precipitation of

unwanted phases (tungsten rich precipitates), coarsening of carbides, alpha phase formation (Cr-rich ferrite) and recrystallization of ferrite grains [10-13]. There are ongoing developments to rise this limit up to ~750°C, e.g., using oxide-dispersion strengthened (ODS) steels containing small amount (about 0.25 wt.%) of homogeneously dispersed nano-size yttria particles [9]. The yttrium-rich nanoparticles effectively suppress softening annealing by blocking dislocations motion at elevated temperatures and recrystallization of ferritic matrix of the steel. In case of HEAs the restricted diffusion due to the distortion of lattice designates their application in this field. However, no detailed study of embrittlement of HEAs after long term operation at high temperature is available. Additionally, introduction of nano-sized oxide particles to the HEA microstructure can overcome the yield strength and the ultimate tensile strength drop at high temperatures and enhance the creep behaviour of HEAs. The ODS steels are usually prepared by powder metallurgy route and yttria particles are introduced to the powder by the mechanical alloying process. Mechanical alloying synthesis and SPS compaction of Al-based Co-Cr-Fe-Ni-Mn-(Ti, Cu, Zn, Mo) one phase FCC or BCC HEAs were reported since 2008 [14-19]. The spontaneous development of strengthening $Cr_{23}C_6$, TiC, Cr-Mn-Fe (σ) phases in the Al-based HEAs during sintering was reported by Fang, Moravcik and Tsai [20-22] accompanied with disintegration of BCC phase onto mixture of Fe-Ni enriched FCC phase and Ni-Al enriched BCC phase after sintering. The preparation of 2 wt.% Al_2O_3 and 0.25 wt.% Y_2O_3 micrometric oxide particles strengthened Al-based Co-Cr-Fe-(Ni, Mn) HEAs by mechanical alloying was reported by Prasad and Praveen [23, 24]. No influence on the phase development and approximately twofold increase in hardness was found in the case of alumina strengthened HEA.

In the present work, we report preparation of an ODS variant of the single FCC phase CoCrFeNiMn HEA strengthened by Y-rich nano particles by the mechanical alloying route. The strengthening effect of nano-sized oxide particles introduced into the microstructure was verified by tensile and creep testing at high operating temperatures.

2. Experimental methods

One phase equiatomic CoCrFeMiMn high entropy alloy was prepared using mechanical alloying method from pure elements (Sigma Aldrich, USA). The 100 g blend of powders was mechanically alloyed using a planetary ball mill (Pulverisette P-6, Fritsch). The milling process was carried out in a hardened steel vial with steel balls for 24 h under vacuum. The ball-to-powder ratio was kept to be 15:1 and rotational speed of a main disc was 350 rpm. The

ODS variant of the HEA (hereafter ODS HEA) was prepared by adding of O_2 gas, Y and Ti to the blend during mechanical alloying. The amount of Y, Ti and O_2 added was fixed to form approximately 0.3 wt.% of oxides in the alloyed powder. The alloyed powders were compacted (SPSed) using spark plasma technique on a TT SPS 10-4 (Thermal Technology LLC, USA) at temperature of 1150°C, pressure of 50 MPa with dwell 5 min and heating/cooling rate 100°C/min. The fully dense pellets with a diameter of 30 mm were machined to the shape appropriate for testing using an electro discharge machining (EDM). A scanning electron microscope LYRA 3 XMU FEG/SEM (Tescan, Czech Republic) equipped with an EDS X-Max80 analyser and an EBSD camera (Oxford Instruments, UK). A transmission electron microscope JEM-2100F (Jeol, Japan) was used for microstructural analyses. The scanning transmission electron microscopy (STEM) mode has been employed in order to characterize the microstructure of the ODS quinary alloy in detail. The TEM worked at the 200 kV accelerating voltage. STEM images were recorded using a High Angular Annular Dark Field detector (HAADF) and the corresponding diffraction patterns were obtained by the conventional TEM Selected Area Diffraction (SAD) technique. Numerical simulations of diffracted intensities were performed by means of a JEMS software [25]. The phase composition was determined on both alloyed powders and SPSed compacts using a X-ray powder diffraction with CoKα radiation (XRD, X´Pert Pro PanAnalytical, The Netherlands). The density of prepared materials was determined using Archimedes method and it was further used for calculation of the elastic modulus using an impulse excitation technique on HT1600 (IMCE, Belgium). Tensile properties were determined at room and 800°C using a flat dog bone shape specimen with nominal cross-section of 0.8 x 3 mm and a gauge length of 10mm. Compression tests were realised at room temperature and at 800°C using cylindrical shape samples with nominal dimensions of 4.5 × 7 mm (d × h). An electromechanical testing system Z50 (Zwick/Roell, Germany) equipped with an atmospheric high temperature furnace MayTec and a high temperature testing system Kappa 100 equipped with a vacuum high temperature furnace (Zwick/Roell, Germany) was employed for tensile and compression testing, respectively. Stress levels between 10 MPa and 30 MPa at temperature of 800°C were tested using a creep mechanical single-lever test machine (IPM, Czech Republic) to evaluate creep resistance. For creep measurement the cylindrical shape samples with dimensions of 5 × 12 mm (d × h) were used. Both creep strain rates and stress creep exponents were determined from recorded creep curves using a CRTES1 software (IPM, Czech Republic).

3. Results and discussion

All elements of the CoCrFeMiMn HEA in powder form (nominally 20 at.% each) were mixed using the ball milling technique and samples of powder were evaluated periodically by the EDS mapping technique. The fully homogenous powder was obtained after 24 hr of milling. The same procedure was applied for ODS HEA. The final composition of powders was checked using the XRD and the resulting spectra can be seen in Fig. 1 showing only one phase composition with nickel based FCC lattice comparable to those found for arc-melted CoCrFeMiMn HEA [26]. There was no observable difference between pure and oxide dispersion strengthened HEA powder. This fact approves the quality of oxide dispersion and its very small size during the ball milling process as is known for ODS steels [27]. Both SPSed and fully dense materials exhibited the identical XRD spectra comparing with initial powders and also between them. It proves the preparation of the one phase FCC alloy.

The density of SPSed HEAs was close to the theoretical density of the CoCrFeNiMn HEA determined as 7.75 g.cm^{-3} (see Table 1). The microstructure of prepared HEA in as received state was found very fine with the medium grain size $d_{50} = 0.8$ μm (see Fig. 2a and Table 1). This is in contrast with the coarse dendritic microstructure obtained by others authors using an arc melting technique [1, 8]. Additionally, no preferably oriented microstructure was observed and confirmed using the EBSD (see Fig. 2b). Significantly finer microstructure was observed for the ODS HEA shown in Fig. 2c where uniform grains having the medium grain size $d_{50} = 0.4$ μm are result of oxides pinning effect.

Results of the STEM - SAD analysis are summarized in Fig. 3. The HAADF image presents a central brighter grain oriented in the <110> FCC axis for the acquisition of a low index SAD pattern. The corresponding SAD data shown in the left inset were obtained from the area delimited by a small circle which represents a position of the SAD aperture during the pattern acquisition. We note that both, the ODS HEA matrix and the central oxide particle contributed to the diffracted electron intensities. These were simulated using a [110] zone orientation for the FCC ODS HEA matrix (cubic Fm-3m, lattice parameter a = 0.360 nm [28]) and the [110] zone orientation for the oxide particle (here we assumed a $CoCr_2O_4$ type of lattice - ICSD structure file no. 61612, cubic Fd-3mZ [29], with a strongly modified lattice parameter a = 2.523 nm). The simulated red diffraction spots were overlaid on the experimental pattern and are presented in the central and right insets for the ODS HEA matrix and the oxide particle, respectively. Places chosen for EDS TEM elemental analysis of matrix (spectrum 1) and oxide nano-particles (spectrum 2 and 3) are visualised in Fig. 3b.

Corresponding EDX spectra and results of quantitative analysis are given in Fig. 3c and Table 2, respectively. The almost nearly equiatomic Co-Cr-Fe-Ni-Mn composition of matrix was proven containing Y_2O_3 precipitates enriched by Ti and other elements from matrix.

Mechanical properties determined on both alloys are summarised in Table 1. The effect of added oxide dispersion to the elastic properties was not significant and the Young's modulus at room temperature was determined on the level of 204.5 ± 0.02 GPa and at 800°C of 133 ± 0.5 GPa for both alloys. Contrary, the tensile behaviour was significantly changed when the oxide dispersion was present in the alloy. Tensile and compression stress-strain curves of HEA and ODS HEA materials, tested at room temperature (RT) and at 800°C, are presented in Fig. 4 and Fig. 5, respectively. The ultimate tensile strength and the yield strength increase of 30% at room temperature and of about 70% at 800°C. The ODS HEA exhibited higher stresses, however, this was compensated by decreasing plasticity. Observed behaviour is typical for alloys with the oxide dispersion as was reported elsewhere [30]. The higher strength of 30% for the ODS HEA at room temperature is probably connected with the finer microstructure resulting in grain boundary strengthening as well as the pinning of dislocation movement on oxides. The formation of twins within larger grains was observed as additional deformation mechanism acting during loading. The presence of nano-metric oxide dispersion inhibits the grain growth and therefore also twining deformation mechanism is suppressed and plastic deformation is limited even at elevated temperatures for the ODS HEA. This phenomenon could explain a widening gap between strength characteristics of the HEA and the ODS HEA with increasing temperature (from 30% at room temperature to 70% at 800°C). The creep experiments were conducted to prove this hypothesis together with the effect of oxide dispersion on creep rates. Temperature of 800°C was selected and secondary creep stadium at various stress levels were evaluated. The creep rates were found one and three orders lower at the stress levels of 10 MPa and 30 MPa, respectively, for the ODS HEA comparing with the HEA as can be deducted from Fig. 6. The slope of the applied stress on the strain rate dependence determines the stress creep exponent which was ~70% lower for the ODS HEA comparing to the HEA which corresponds well with tensile results.

4. Conclusion

In summary, the feasibility of the yttria nano-oxide dispersion strengthened one phase FCC CoCrFeNiMn high entropy alloy preparation by the mechanical alloying followed by in-situ oxides precipitation was confirmed in this study. The introduction of nano-oxides in to the

HEA microstructure resulted in the presence of effective grain boundary and dislocation pinning effects. The ODS HEA exhibited 50% grain size reduction to the size under 500 nm. The ultimate tensile strength and the yield strength of the ODS HEA increased of 30% at room temperature and of about 70% at 800°C. The creep strain rates for the ODS HEA were significantly lower, i.e., three orders lower for 30MPa stress level, compared with the non-ODS HEA.

Acknowledgement

References

[1] B. Cantor, I.T.H. Chang, P. Knight, A.J.B. Vincent, Microstructural development in equiatomic multicomponent alloys, Materials Science and Engineering: A 375–377 (2004) 213-218.

[2] J.W. Yeh, S.K. Chen, S.J. Lin, J.Y. Gan, T.S. Chin, T.T. Shun, C.H. Tsau, S.Y. Chang, Nanostructured High-Entropy Alloys with Multiple Principal Elements: Novel Alloy Design Concepts and Outcomes, Advanced Engineering Materials 6(5) (2004) 299-303.

[3] A. Gali, E.P. George, Tensile properties of high- and medium-entropy alloys, Intermetallics 39 (2013) 74-78.

[4] K.Y. Tsai, M.H. Tsai, J.W. Yeh, Sluggish diffusion in Co–Cr–Fe–Mn–Ni high-entropy alloys, Acta Materialia 61(13) (2013) 4887-4897.

[5] M.-H. Tsai, J.-W. Yeh, High-Entropy Alloys: A Critical Review, Materials Research Letters 2(3) (2014) 107-123.

[6] B. Gludovatz, A. Hohenwarter, D. Catoor, E.H. Chang, E.P. George, R.O. Ritchie, A fracture-resistant high-entropy alloy for cryogenic applications, Science 345(6201) (2014) 1153-1158.

[7] R. Carroll, C. Lee, C.-W. Tsai, J.-W. Yeh, J. Antonaglia, B.A.W. Brinkman, M. LeBlanc, X. Xie, S. Chen, P.K. Liaw, K.A. Dahmen, Experiments and Model for Serration Statistics in Low-Entropy, Medium-Entropy, and High-Entropy Alloys, Scientific Reports 5 (2015) 16997.

[8] F. Otto, A. Dlouhý, C. Somsen, H. Bei, G. Eggeler, E.P. George, The influences of temperature and microstructure on the tensile properties of a CoCrFeMnNi high-entropy alloy, Acta Materialia 61(15) (2013) 5743-5755.

[9] S.J. Zinkle, N.M. Ghoniem, Operating temperature windows for fusion reactor structural materials, Fusion Engineering and Design 51–52 (2000) 55-71.

[10] P. Fernández, A.M. Lancha, J. Lapeña, M. Serrano, M. Hernández-Mayoral, Metallurgical properties of reduced activation martensitic steel Eurofer'97 in the as-received condition and after thermal ageing, Journal of Nuclear Materials 307–311, Part 1 (2002) 495-499.

[11] P. Fernández, M. García-Mazarío, A.M. Lancha, J. Lapeña, Grain boundary microchemistry and metallurgical characterization of Eurofer'97 after simulated service conditions, Journal of Nuclear Materials 329–333, Part A (2004) 273-277.

[12] J.S. Lee, C.H. Jang, I.S. Kim, A. Kimura, Embrittlement and hardening during thermal aging of high Cr oxide dispersion strengthened alloys, Journal of Nuclear Materials 367–370, Part A (2007) 229-233.

[13] H. Hadraba, I. Dlouhy, Effect of thermal ageing on the impact fracture behaviour of Eurofer'97 steel, Journal of Nuclear Materials 386–388 (2009) 564-568.

[14] S. Varalakshmi, M. Kamaraj, B.S. Murty, Synthesis and characterization of nanocrystalline AlFeTiCrZnCu high entropy solid solution by mechanical alloying, Journal of Alloys and Compounds 460(1–2) (2008) 253-257.

[15] S. Varalakshmi, M. Kamaraj, B.S. Murty, Processing and properties of nanocrystalline CuNiCoZnAlTi high entropy alloys by mechanical alloying, Materials Science and Engineering: A 527(4–5) (2010) 1027-1030.

[16] Y.-L. Chen, Y.-H. Hu, C.-A. Hsieh, J.-W. Yeh, S.-K. Chen, Competition between elements during mechanical alloying in an octonary multi-principal-element alloy system, Journal of Alloys and Compounds 481(1–2) (2009) 768-775.

[17] W. Chen, Z. Fu, S. Fang, H. Xiao, D. Zhu, Alloying behavior, microstructure and mechanical properties in a FeNiCrCo0.3Al0.7 high entropy alloy, Materials & Design 51 (2013) 854-860.

[18] C. Wang, W. Ji, Z. Fu, Mechanical alloying and spark plasma sintering of CoCrFeNiMnAl high-entropy alloy, Advanced Powder Technology 25(4) (2014) 1334-1338.

[19] W. Ji, Z. Fu, W. Wang, H. Wang, J. Zhang, Y. Wang, F. Zhang, Mechanical alloying synthesis and spark plasma sintering consolidation of CoCrFeNiAl high-entropy alloy, Journal of Alloys and Compounds 589 (2014) 61-66.

[20] S. Fang, W. Chen, Z. Fu, Microstructure and mechanical properties of twinned Al0.5CrFeNiCo0.3C0.2 high entropy alloy processed by mechanical alloying and spark plasma sintering, Materials & Design (1980-2015) 54 (2014) 973-979.

[21] I. Moravcik, J. Cizek, P. Gavendova, S. Sheikh, S. Guo, I. Dlouhy, Effect of heat treatment on microstructure and mechanical properties of spark plasma sintered AlCoCrFeNiTi0.5 high entropy alloy, Materials Letters 174 (2016) 53-56.

[22] M.-H. Tsai, H. Yuan, G. Cheng, W. Xu, W.W. Jian, M.-H. Chuang, C.-C. Juan, A.-C. Yeh, S.-J. Lin, Y. Zhu, Significant hardening due to the formation of a sigma phase matrix in a high entropy alloy, Intermetallics 33 (2013) 81-86.

[23] H. Prasad, S. Singh, B.B. Panigrahi, Mechanical activated synthesis of alumina dispersed FeNiCoCrAlMn high entropy alloy, Journal of Alloys and Compounds 692 (2017) 720-726.

[24] S. Praveen, A. Anupam, T. Sirasani, B.S. Murty, R.S. Kottada, Characterization of Oxide Dispersed AlCoCrFe High Entropy Alloy Synthesized by Mechanical Alloying and Spark Plasma Sintering, Transactions of the Indian Institute of Metals 66(4) (2013) 369-373.

[25] P.A. Stadelmann, JEMS e Electron Microscopy Software, Version

4.2231U2014, Copyright P. Stadelmann 1999-2014, JEMS-SAAS, Switzerland, 2014.

[26] P.P. Bhattacharjee, G.D. Sathiaraj, M. Zaid, J.R. Gatti, C. Lee, C.-W. Tsai, J.-W. Yeh, Microstructure and texture evolution during annealing of equiatomic CoCrFeMnNi high-entropy alloy, Journal of Alloys and Compounds 587 (2014) 544-552.

[27] H. Xu, Z. Lu, D. Wang, C. Liu, Microstructural evolution in a new Fe based ODS alloy processed by mechanical alloying, Nuclear Materials and Energy 7 (2016) 1-4.

[28] G. Laplanche, P. Gadaud, O. Horst, F. Otto, G. Eggeler, E.P. George, Temperature dependencies of the elastic moduli and thermal expansion coefficient of an equiatomic, single-phase CoCrFeMnNi high-entropy alloy, Journal of Alloys and Compounds 623 (2015) 348-353.

[29] P. García Casado, I. Rasines, Preparation and crystal data of the spinel series Co1+2sCr2−3sSbsO4 (O ⩽ s ⩽ 23), Polyhedron 5(3) (1986) 787-789.

[30] D.T. Hoelzer, J. Bentley, M.A. Sokolov, M.K. Miller, G.R. Odette, M.J. Alinger, Influence of particle dispersions on the high-temperature strength of ferritic alloys, Journal of Nuclear Materials 367–370, Part A (2007) 166-172.
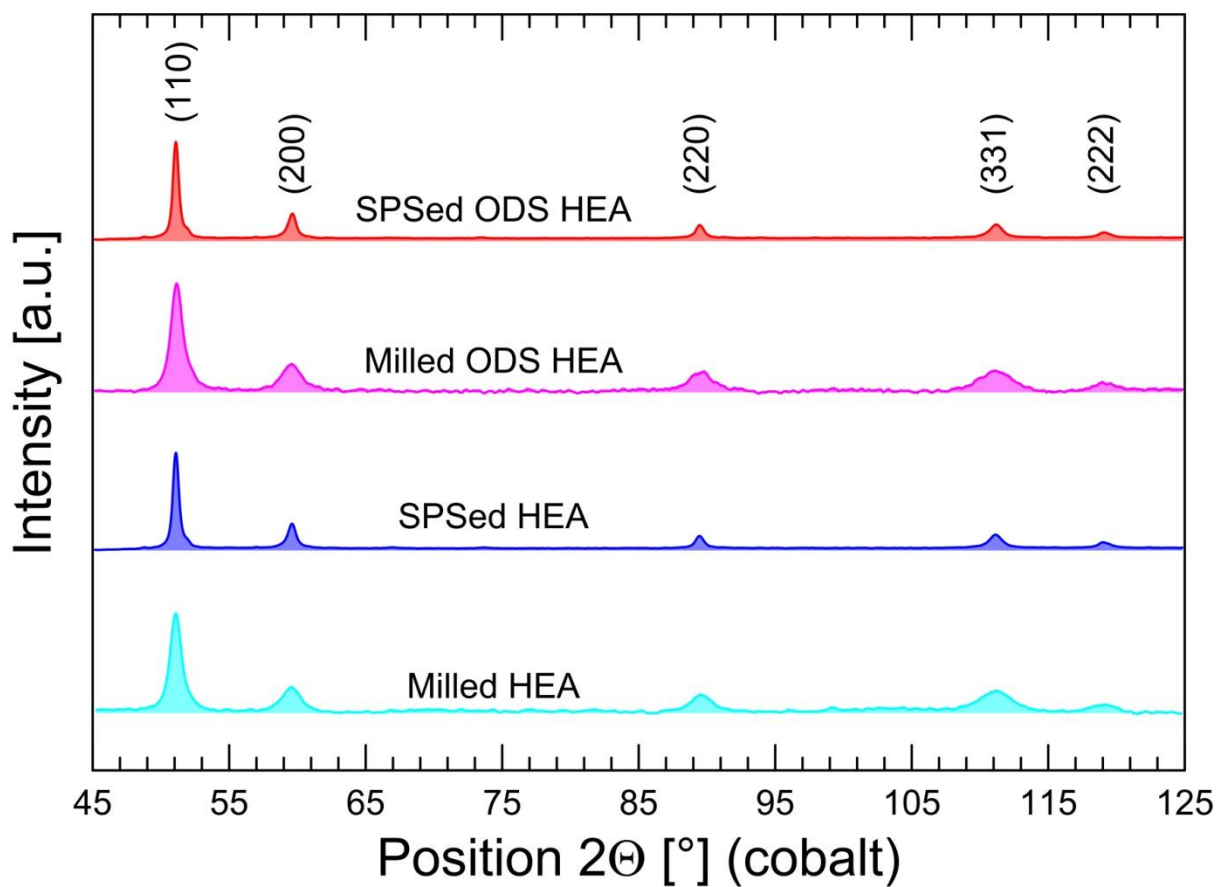
Fig. 1 XRD patterns of HEA and ODS HEA alloyed powders and SPSed compacts.
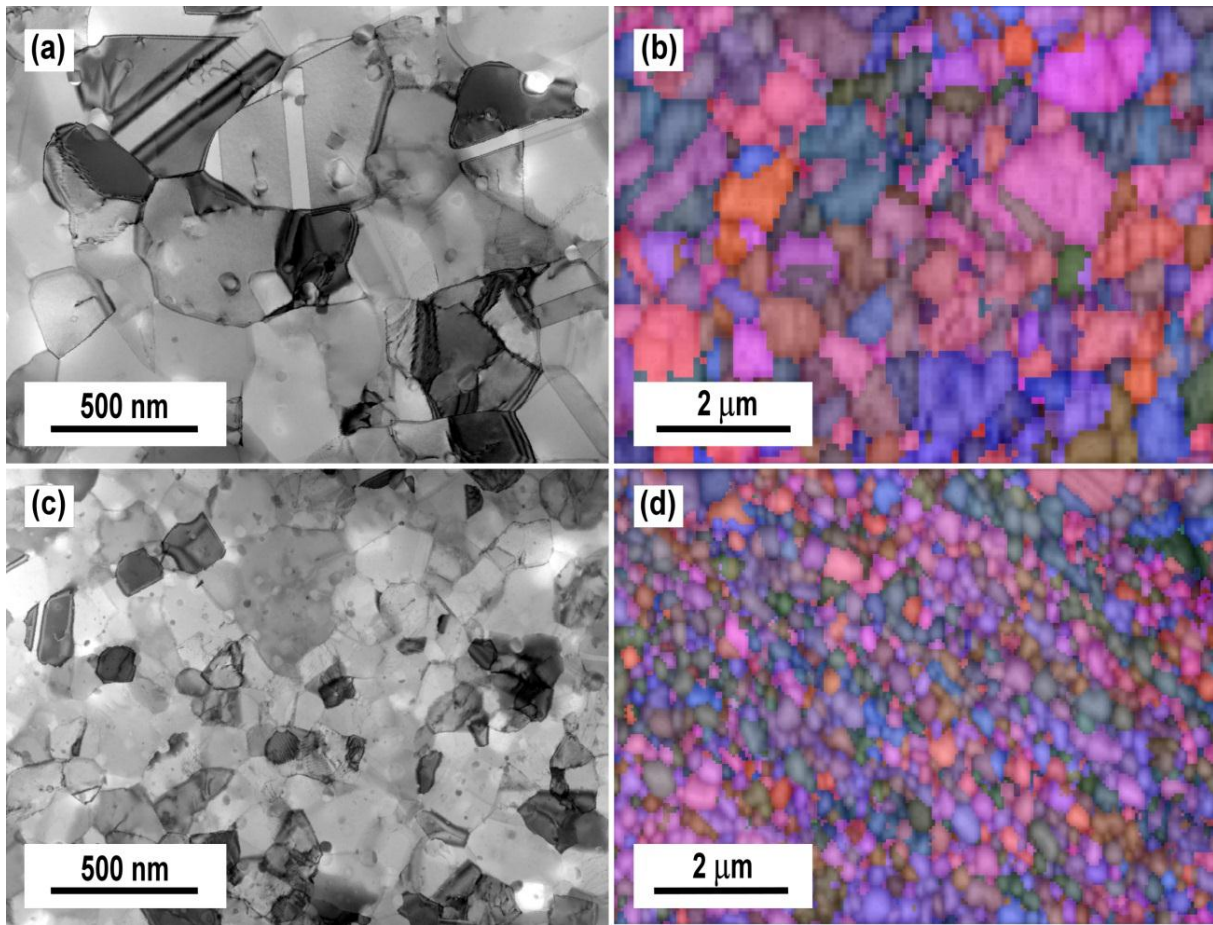
ACCEPTED MANUSCRIPT

Fig. 2 Grain structure of SPSed HEA (up) and ODS HEA (down) visualised by STEM (left) and EBSD SEM (right).
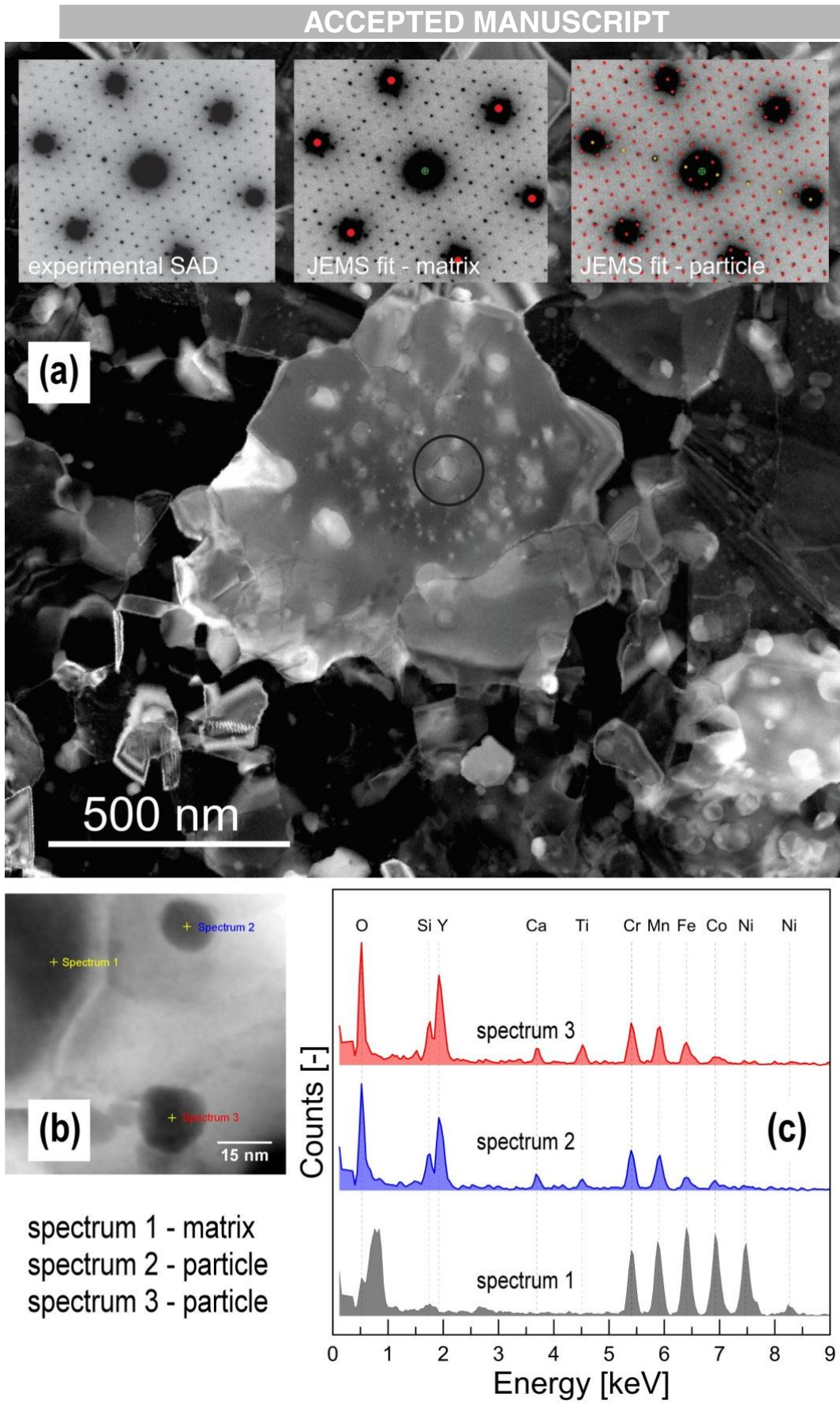
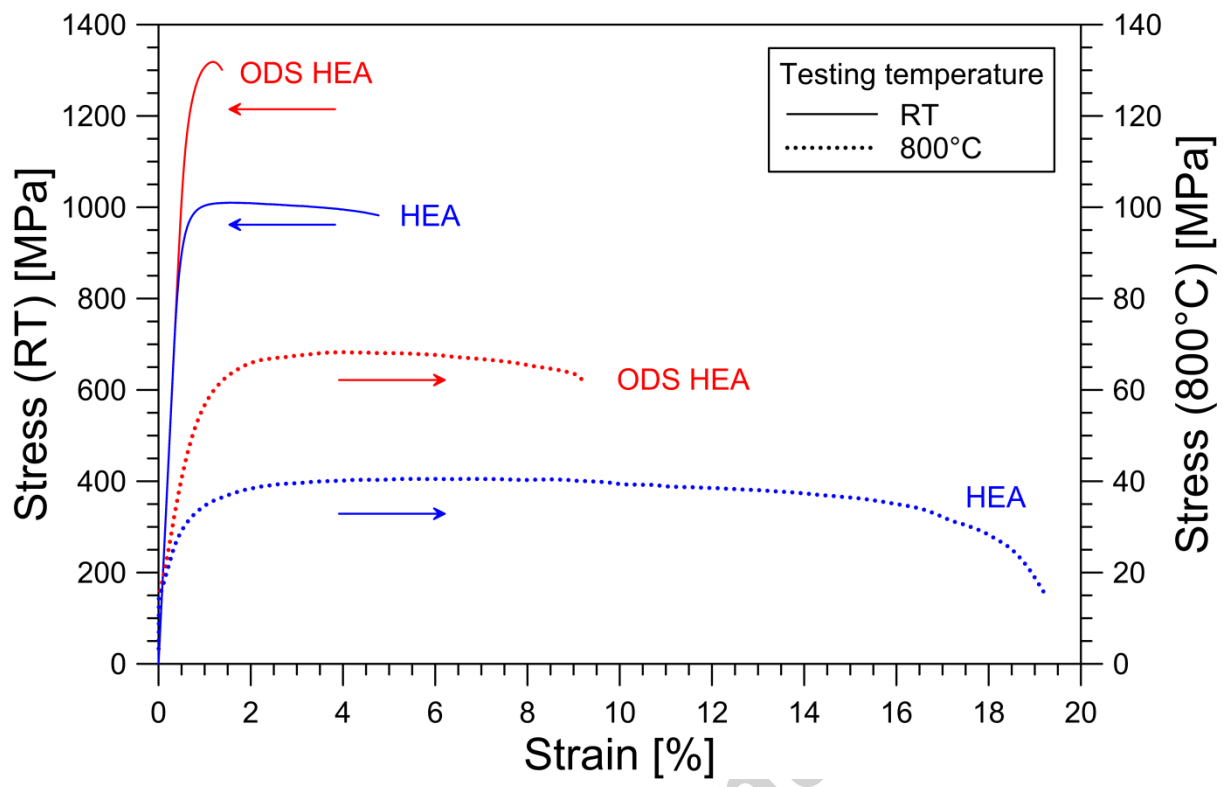Fig. 3 STEM - SAD and EDS analysis of oxide dispersion in ODS HEA.

Fig. 4 Tensile stress-strain curves of HEA and ODS HEA tested at room temperature (RT) and at 800°C.
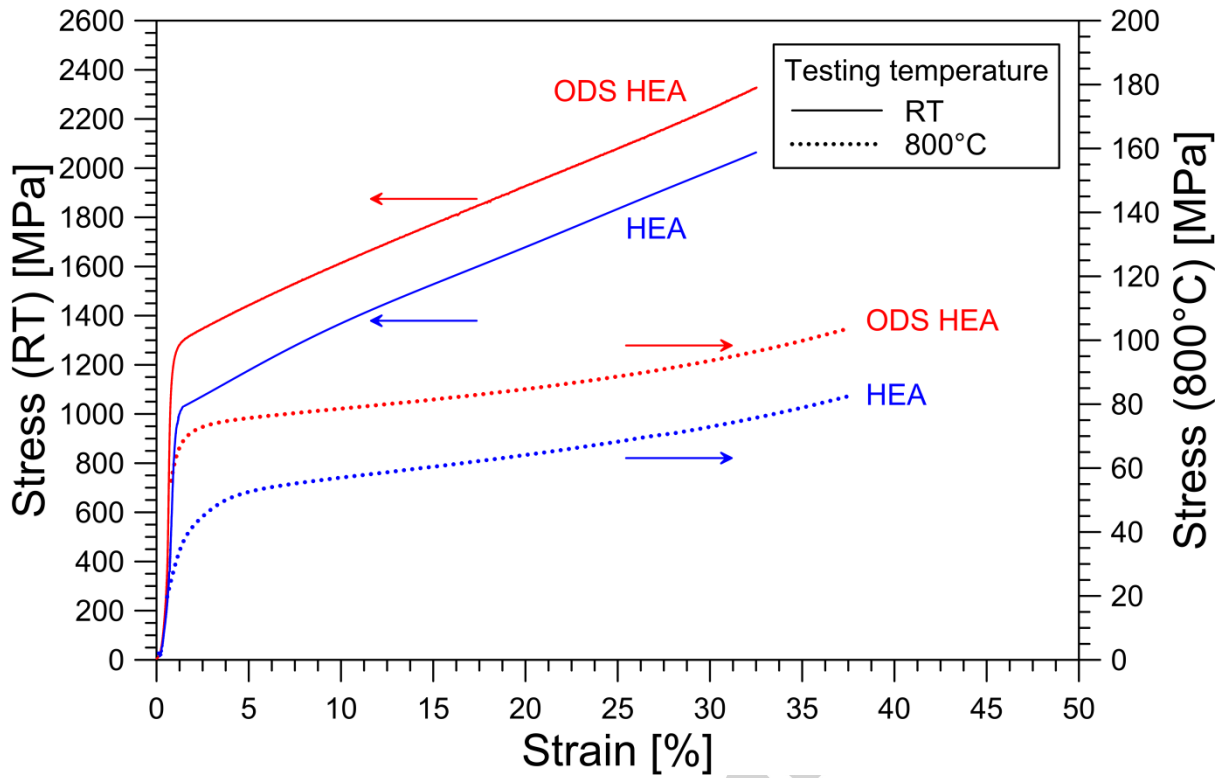
Fig. 5 Compression stress-strain curves of HEA and ODS HEA tested at room temperature (RT) and at 800°C.

ACCEPTED MANUSCRIPT

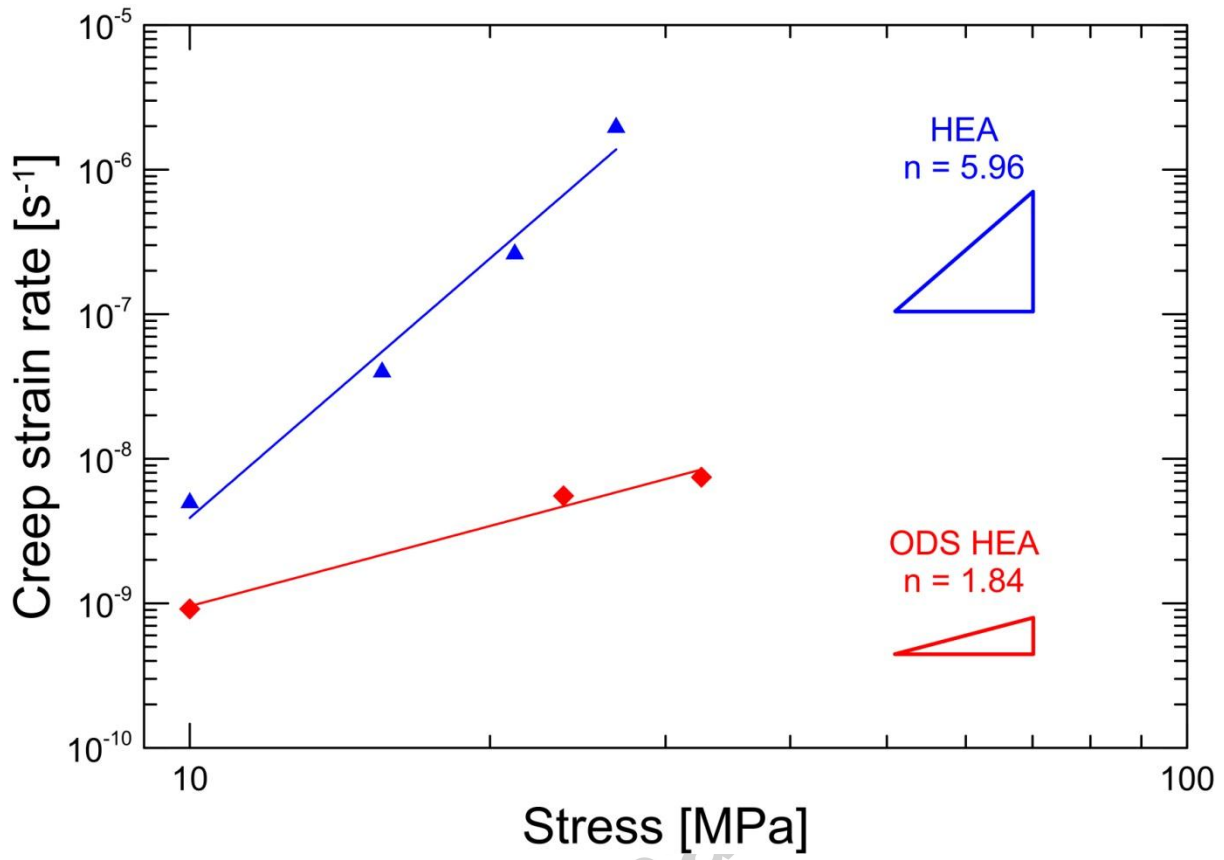
Fig. 6 Dependence of minimum creep rate for HEA and ODS HEA on applied stress (tested at 800°C).

ACCEPTED MANUSCRIPT

Table 1 Density, grain size and mechanical properties of SPSed HEA and ODS HEA.

		tested at RT			tested at 800°C		
		HEA	ODS HEA	percentual change	HEA	ODS HEA	percentual change
density	(g.cm^{-3})	7.76	7.71	none	n.a.	n.a.	n.a.
d_{50}	(μm)	0.8	0.4	-50%	n.a.	n.a.	n.a.
HV0.1(≈1N)	(GPa)	3.63	4.24	+24%	n.a.	n.a.	n.a.
E	(GPa)	204	204	none	133	133	none
σ_{Yt}	(MPa)	971	1269	+30%	31.5	55	+75%
σ_{Yc}	(MPa)	1005	1232	+30%	37	62	+68%
σ_{UTS}	(MPa)	1010	1318	+30%	40.5	68	+68%
elongation	(%)	4.29	0.74	-83%	18.82	9.3	-51%
stress creep exponent	(s^{-1})	n.a.	n.a.	n.a.	5.96	1.84	-69%

RT − room temperature (22°C), d_{50} − median grain size, HV0.1 − Vickers hardness at load 0.1 kg, E − Young´s modulus; σ_{Yt}, σ_{Yc} − yield strength in tension and compression; respectively and σ_{UTS} − ultimate tensile strength, n.a. − not analysed.

Table 2 Chemical composition of analysed places determined by EDS in at.%.

Element	Co	Cr	Fe	Ni	Mn	Y	O	Ti
Spectrum 1	22.14	16.62	23.7	20.43	17.74	0.00	n.a.	0.00
Spectrum 2	2.7	10.7	3.5	0.76	7.28	23.83	50.90	2.4
Spectrum 3	1.49	8.43	4.39	0.38	7.61	23.95	50.14	3.60